Supporting Information

Phonon polaritons in van der Waals polar heterostructures for broadband strong light-matter interactions

Tianwei Qin[1,2], *Weiliang Ma*[1,2], *Tao Wang*[3]*, *Peining Li*[1,2]*

Affiliations:

[1]Wuhan National Laboratory for Optoelectronics and School of Optical and Electronic Information, Huazhong University of Science and Technology; Wuhan, 430074, China.

[2]Optics Valley Laboratory; Hubei, 430074, China.

[3]Institute of Functional Nano & Soft Materials (FUNSOM), Jiangsu Key Laboratory for Carbon-Based Functional Materials & Devices, Soochow University, 199 Ren'ai Road, Suzhou, 215123, Jiangsu, China.

*Corresponding author. Email: wangtao2019@suda.edu.cn, lipn@hust.edu.cn

Note S1. Dielectric function of materials

A. Permittivity of h-BN

Isotopically (^{10}B) enriched h-BN was used during sample fabrications. The permittivity tensor of h-BN is modelled as follows:

$$\varepsilon_j = \varepsilon_{\infty,j}\left(1 + \frac{\omega_{LO,j}^2 - \omega_{TO,j}^2}{\omega_{TO,j}^2 - \omega^2 - i\omega\gamma_j}\right) \#(1)$$

where $j = \perp, \parallel$ denotes the direction of the tensor component perpendicular or parallel the optic axis. Hence $\varepsilon_\perp$and ε_{II} represent in-plane and out-plane permittivity. Parameters are taken from ref 1 except $\varepsilon_{\infty,\perp}$, which was changed to 4.5 cm^{-1} instead of 5.1 cm^{-1} for best matching between simulations and experiments. Table S1 below shows all parameters of the dielectric function.

Supplementary Table S1. Parameters of the h-BN dielectric function. All parameters are expressed in cm^{-1} except for ε_∞.

j	ω_{TO}	ω_{LO}	γ	ε_∞
$\perp$	1394.5	1650	1.8	4.5
$\parallel$	785	845	1	2.5

B. Permittivity of α-MoO_3

Due to anisotropy of α-MoO_3, components of the permittivity tensor are defined as ε_x, ε_y and ε_z, in which x, y and z correspond to crystalline directions of α-MoO_3, [100], [001], and [010], respectively. The dielectric function of α-MoO_3 is described by Lorentz model as shown in ref 2.

C. Permittivity of α-quartz

As a uniaxial crystal, α-quartz exhibits weak hyperbolicity. Its permittivity tensor is comprised of $\varepsilon_\perp$and ε_{II}, which represent the component direction perpendicular or parallel the optic axis. Each component of the tensor can be modelled according to following formula:

$$\varepsilon_{quartz} = \varepsilon_{\infty} \prod_{j} \frac{\omega_{LO_j}^2 - \omega^2 - i\gamma_{LO_j}\omega}{\omega_{TO_j}^2 - \omega^2 - i\gamma_{TO_j}\omega} \#(2)$$

where j marks the vibrational mode index of phonon. When quartz and α-MoO_3 are assembled together, it is noted that quartz's optic axis was placed parallel to [001] of α-MoO_3. All parameters for the permittivity function were from ref 3 and presented in table S2.

Supplementary Table S2. Parameters of the α-quartz dielectric function. All parameters are expressed in cm^{-1} except for ε_{∞}.

	j	ω_{TO}	γ_{TO}	ω_{LO}	γ_{LO}	ε_{∞}
$\varepsilon_{\perp}$	1	796.5	6.0	809.1	5.2	2.296
$\varepsilon_{\perp}$	2	1063.0	7.1	1230.0	12.1	
$\varepsilon_{\perp}$	3	1157.0	7.2	1154.8	6.3	
$\varepsilon_{\parallel}$	1	775.3	5.9	788.8	6.8	2.334
$\varepsilon_{\parallel}$	2	1070.9	5.3	1239.6	11.5	

D. Permittivity of molecules used in simulations

As for simulations in Figure 4, we assumed a given molecule with 3 vibrational modes. Its permittivity is modelled as the sum of a non-dispersive background and Lorentz oscillators which describe molecular vibrations:

$$\varepsilon = \varepsilon_{\infty} + \sum_{k} \frac{S_k^2}{\omega_k^2 - \omega^2 - i\omega\gamma_k} \#(3)$$

where k indicates the oscillator index. Parameters for dielectric function of the molecule are shown in table S3. Note that intensity and damping of the given molecule's oscillator refer to the molecular vibration at 1450 cm^{-1} of CBP.

Supplementary Table S3. Parameters for dielectric function of the given molecule. All parameters are expressed in cm^{-1} except for ε_{∞}.

k	ω_k	S_k	γ_k	ε_∞
1	1450	128	6.4	2.8
2	1136	128	6.4	
3	870	128	6.4	

Note S2. Infrared optical imaging

A. Reflection spectra and simulations

We measured far-field reflection spectra in the heterostructure area under two polarizations either parallel (P0˚) or perpendicular (P90˚) to the α-MoO_3 crystal direction[100]. The far-field reflection spectra were measured with a commercial Bruker-LUMOS II Fourier transform infrared (FTIR) spectrometer. The incident angle of the TM polarized illumination is around 30°, then reflected by the sample. The consequent reflection spectra are recorded by the mercury cadmium telluride (MCT) detector. The reflectance spectra in Figure 1d were acquired with the aperture set to 20 × 20 μm^2, in reference to a clean gold substrate at same conditions. Corresponding simulations calculated by transfer matrix method are shown in Figure S1.

Narrow peak A2 and A4 are induced by TO phonon of thin α-MoO_3 and hBN flake respectively. Phonons in quartz lead to broad peak A3, B2 and small peak A1, B1. Weak anisotropy of quartz can be identified by comparing intensity of the dip inside A3 and B2. We note that in FigureS1.b, the dip appears in the experiment but totally disappears in the simulation. That's because during FTIR experiments, we used a microscope with focused illumination which could couple with the out-of-plane phonons. However, in simulations, the propagation direction of the incident light is assumed strictly normal to the substrate. A4 and B3 located in the same wavenumber verify in-plane isotropy of hBN, while the vanishment of A2 in FigureS1.b manifests strong hyperbolicity of α-MoO_3.

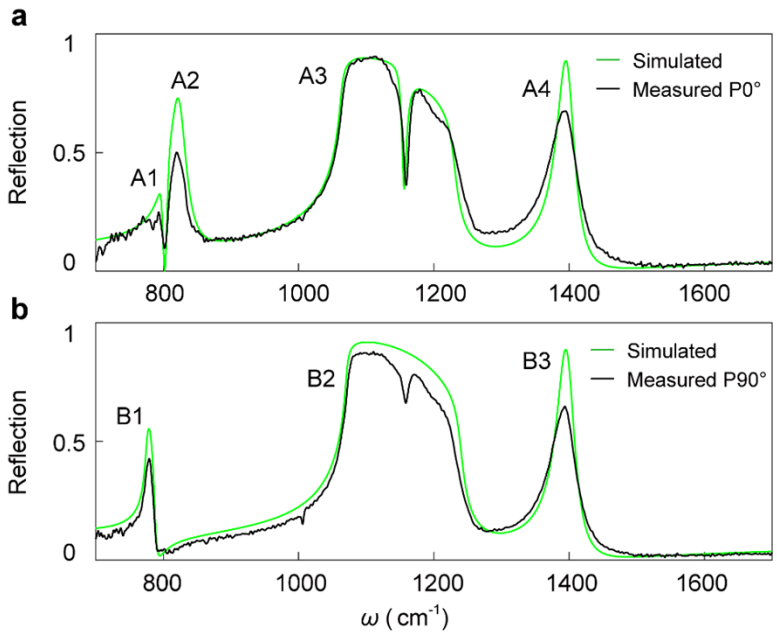

Supplementary Figure S1. FTIR-measured (black lines) and simulated (green lines) spectra of the heterostructure area for different polarizations. Simulations are performed by transfer matrix method.

B. Theoretical electric field distribution

Figure S2 presents electromagnetic field distribution of phonon polaritons (PhPs) in h-BN-α-MoO_3-quartz stacking layers. It reveals highly confined PhPs inside hBN and α-MoO_3, and SPhPs propagating on the surface of quartz. Colored lines indicate intensity of E_z which decays to 1/e from maximum along vertical direction. It is observed that sufficient electromagnetic signals propagate to the top of heterostructure, thus detected by a near-field tapping tip of s-SNOM.

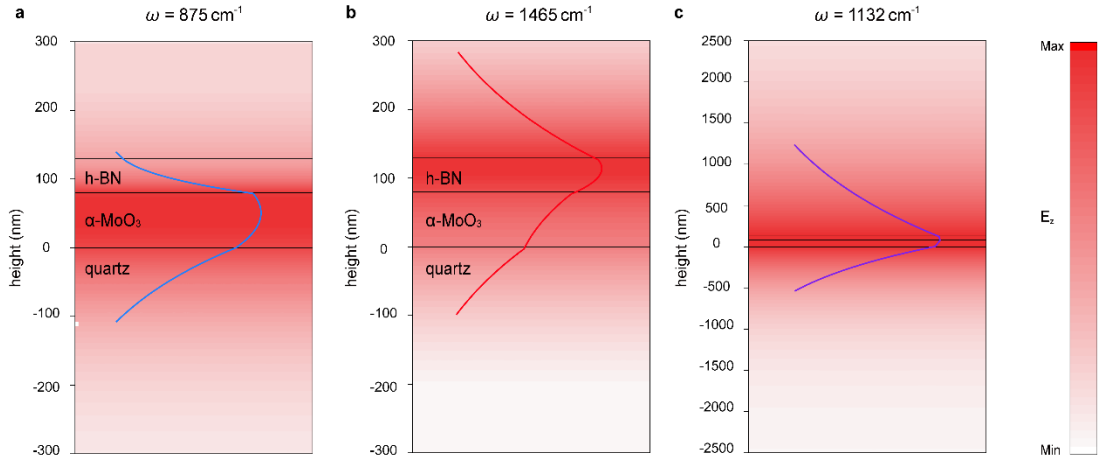

Supplementary Figure S2. Simulated electric field distribution E_z of hBN-α-MoO_3-quartz heterostructure at ω=875, 1465, 1132 cm^{-1}. Curves which superimposed on color plots are calculated E_z along height direction, and end at points where the intensity decays to 1/*e* of the maximum. Layer thicknesses of h-BN and α-MoO_3 are set to 50 nm and 80 nm.

C. Fitting procedure for line profiles of PhPs

To obtain real and imaginary part of wavevectors for propagating PhPs[4] (Figure 2g-i in the main text), we expressed the near-field interferometry signals as a function of distance *x*:

$$\mathrm{Re}\,(S(x)) = S_0 + A\frac{e^{\frac{-2x}{L}}}{\sqrt{x}}\sin\frac{4\pi(x-x_c)}{\lambda_p} + B\frac{e^{-\frac{x}{L}}}{x}\sin\frac{2\pi\left(x-x_c^{'}\right)}{\lambda_p} \#(4)$$

where L and λ_p represent propagation length and polariton wavelength, x_c and x_c' are phase shift. The equation includes the background signal S_0, tip and edge-launched PhPs (A and B are parameters for tip and edge-launched PhPs). After using the above equation to fit line profiles extracted from interferometry images, we can get real part of propagation wavevectors by $\mathrm{Re}(k)=2\pi/\lambda_p$, imaginary part by $\mathrm{Im}(k)=1/L$.

Supplementary Table S4 shows fitting parameters of propagating PhPs in the heterostructure corresponding to Figure. 2g-i. A/B indicates the ratio of tip-launched and edge-launched PhPs. As shown in Supplementary Table S4, PhPs are mainly excited by the tip at ω = 1000 cm^{-1} and 1465 cm^{-1}. At ω = 870 cm^{-1}, PhPs are mostly excited by the

edge due to the low laser energy when the incident light frequency is close to the cutoff frequency of quantum cascade laser (QCL).

Supplementary Table S4. Fitting parameters S_0 and A/B of propagating PhPs in the heterostructure corresponding to Figure. 2g-i.

ω	870 cm^{-1}	1000 cm^{-1}	1465 cm^{-1}
S_0 (a.u.)	0.89	0.85	0.35
A/B	0.0001	850	630

D. Optical losses of the stacking device

Optical loss can be assessed by the figure of merit (FOM) dependent of polariton wavevector: FOM = q / γ, where q and γ indicate the real part and imaginary part of the wavevector. Supplementary table S1 compares FOM of PhPs in the heterostructure with it in individual hBN or α-MoO_3. The comparison suggests that not much polariton damping is caused by vdW-layer stack and assembly, revealing the excellent property of PhPs inside our stacking device.

Supplementary Table S5. FOM of PhPs in the heterostructure or individual hBN and α-MoO_3, at 870, 1000 and 1465 cm^{-1}. FOMs of heterostructure are extracted from fitting results of experimental data (Figure 2g-i in the main text), and FOMs in individual materials are calculated from simulations (Thicknesses of hBN and α-MoO_3 are 50nm and 80nm).

	FOM (q+iγ)		
ω	870 cm^{-1}	1000 cm^{-1}	1465 cm^{-1}
Individual material	12(4.1+0.3i)	8(24.8+3.2i)	62(3.5+0.1i)
Heterostructure	10(12.4+1.2i)	8(6.8+0.9i)	45(6.6+0.2i)

E. PhPs on van der Waals heterostructures with different material layers

From the supplementary figure S3.d-f, we extracted line profiles of two areas: three-layer structure of hBN/α-MoO_3/quartz (solid line) and double-layer structure of α-MoO_3/quartz

or hBN/quartz (dashed line) (Figure. 2g-i). PhPs on both areas are launched by the same edge but exhibiting totally different propagation wavevectors. That's because they exist in different dielectric environment, which caused by distinct stacking structures on these two areas. It's noted that the wavevector of PhPs propagating inside crystals can be tuned by changing materials above or below.

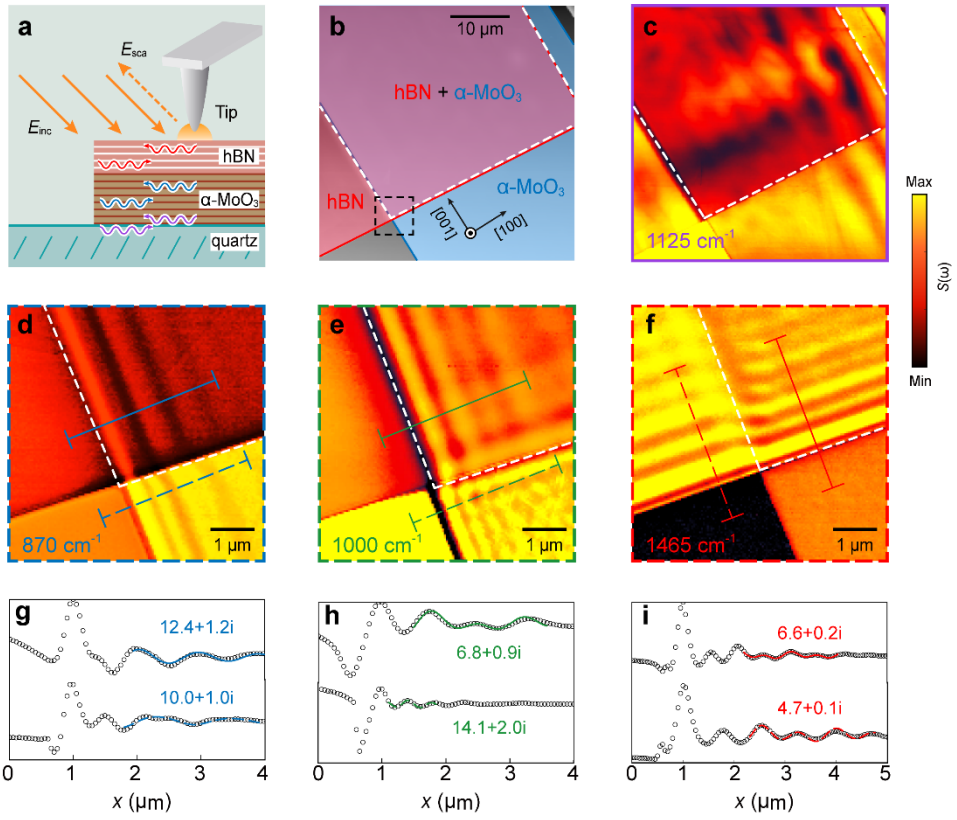

Supplementary Figure S3. Real-space imaging of phonon polaritons on the h-BN-MoO3-quartz heterostructure. (a) Schematic of the s-SNOM nanoimaging experiment. Orange arrows denote illumination of the sample edge and tip-scattered radiation. Red, blue and purple arrows illustrate the PhPs propagating on h-BN, MoO3 and quartz respectively. (b) Topography image of the heterostructure. Red and blue region mark h-BN flake (thickness is 50nm) and MoO3 flake (thickness is 80nm). (c-f) Infrared near-field amplitude images taken at 1125 cm^{-1} ,870 cm^{-1} ,1000 cm^{-1} and 870 cm^{-1}. (c) was taken at the frequency within quartz RB, as (d) and (e) at α-MoO_3 RB, (f) at hBN RB. Scan areas of (d)-(f) are marked as the black dotted box in (b). (g-i) Normalized amplitude profiles extracted along

the solid or dashed lines in (d) to (f) respectively. Their corresponding fitting results are plotted as colored lines, with fitting wavevectors marked beside.

Note S3. Details for Figure 4

A. Mode solver VS transfer matrix

When analyzing interactions between PhPs and molecular vibrations (Figure 4c-f), the spatial dispersion can be found using transfer-matrix method or mode solver in COMSOL. Figure S3 present the spatial dispersion calculated by these two methods. Both dots and the line exhibit back bending around the molecular vibration, and nearly consistent trend.

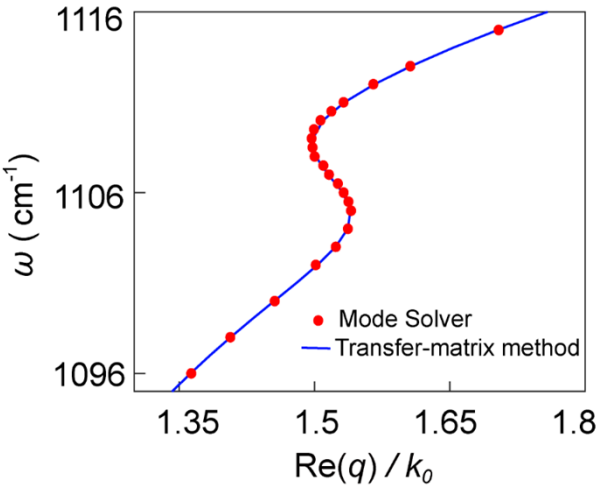

Supplementary Figure S4. The spatial dispersion in Figure 4d of main text calculated by two methods. Blue line shows results calculated by transfer-matrix method when assuming real-valued wavenumber and complex-valued wavevector, while red dots are simulated by mode solver.

B. Eigenmode analysis in RB of quartz, h-BN and α-MoO_3

We apply eigenmode analysis[5] to study the coupling between PhPs in quartz, h-BN and α-MoO_3 and multiple molecular vibrations (Figure S4). The thickness-tuning mode splitting illustrated in Figure S4, manifest good consistence with the principle in Figure 4c-d of the main text.

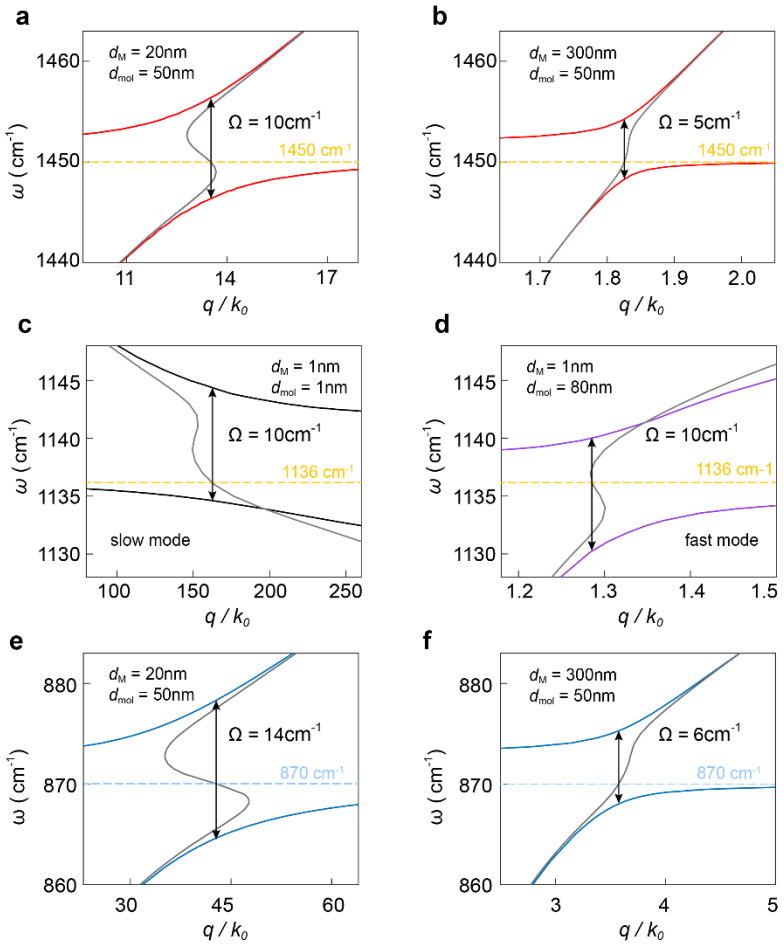

Supplementary Figure S5. Dispersions of PhPs for vdW layer with various thicknesses, calculated by transfer matrix method assuming complex momenta (grey lines) or complex frequencies (purple lines). Horizontal dashed lines mark the frequency of the molecular vibrational resonances.

C. Determination of strong coupling region

To obtain linewidth of PhPs, we model heterostructure structure as Figure 4a of main text, but without molecular vibration part in dielectric function. Under such uncoupled PhP mode, we calculate eigenmodes assuming real momenta and complex frequency. The imaginary part of the complex-valued frequency is equal to half linewidth of PhPs (l_{PhP}). Note that little change occurred for linewidth of PhPs in different-thickness vdW layers. We choose l_{PhP} in the worst scenario when layer thickness is 20 nm.

A strict condition is widely used to confirm strong coupling of a system:

$$C = \frac{\Omega^2}{{l_{PhP}}^2/2 + {l_{mol}}^2/2} > 1 \#(5)$$

where l_{mol} is equal to the oscillator damping of the considered molecular vibration. Values of l_{mol} and l_{PhP} used in calculations are presented in Supplementary Table S2.

Supplementary Table S6. l_{mol} and l_{PhP} used in calculations of coupling condition C, for molecular vibrations at 1136 cm^{-1}, 870 cm^{-1}, and 1450 cm^{-1}.

molecular vibration	l_{mol} (cm^{-1})	l_{PhP} (cm^{-1})
1450 cm^{-1}	6.4	1.9
1136 cm^{-1}	6.4	7 (fast mode)
	6.4	7.5(slow mode)
870 cm^{-1}	6.4	5.2

References for Supporting Information:

1. A. J. Giles, S. Dai, I. Vurgaftman, T. Hoffman, S. Liu, L. Lindsay, C. T. Ellis, N. Assefa, I. Chatzakis, T. L. Reinecke, J. G. Tischler, M. M. Fogler, J. H. Edgar, D. N. Basov and J. D. Caldwell, *Nat. Mater.*, 2018, **17**, 134-139.
2. G. Álvarez-Pérez, T. G. Folland, I. Errea, J. Taboada-Gutiérrez, J. Duan, J. Martín-Sánchez, A. I. Tresguerres-Mata, J. R. Matson, A. Bylinkin, M. He, W. Ma, Q. Bao, J. I. Martín, J. D. Caldwell, A. Y. Nikitin and P. Alonso-González, *Adv. Mater.*, 2020, **32**, 1908176.
3. C. J. Winta, M. Wolf and A. Paarmann, *Phys. Rev. B: Condens. Matter*, 2019, **99**, 144308.
4. Y. Wu, Q. Ou, Y. Yin, Y. Li, W. Ma, W. Yu, G. Liu, X. Cui, X. Bao, J. Duan, G. Á.-P. Z. Dai, B. Shabbir, N. Medhekar, X. Li, C.-M. Li, P. Alonso-González and Q. Bao, *Nat. Commun.*, 2020, **11**, 2646.
5. A. Bylinkin, M. Schnell, M. Autore, F. Calavalle, P. Li, J. Taboada-Gutierrez, S. Liu, J. H. Edgar, F. Casanova, L. E. Hueso, P. A.-G. A. Y. Nikitin and R. Hillenbrand, *Nat. Photonics*, 2021, **15**, 197-202.